Prepared for:

Wintershall Noordzee B.V.
Eisenhowerlaan 142
2517 KN Den Haag
Nederland

Final Report

SPECIAL CORE ANALYSIS

on Core 1 from WELL D12-A2

By Stefano Pruno

Reviewed by Albert Hebing

Report No. c0312

February 2005

Wintershall Noordzee B.V.
Eisenhowerlaan 142
2517 KN Den Haag
The Nederlands

Attention: Mr. B. De Wijn

Leiderdorp, February 2005

Subject: Special core analysis study - Well D12-A2

Dear Mr. B. De Wijn,

Presented are four copies of the final report "Special Core Analysis on Core 1 from Well D12-A2". The services here reported were performed in accordance with instructions received from Wintershall Noordzee B.V

It has been a pleasure to perform this study for Wintershall Noordzee B.V. and please do not hesitate to contact us if you need more information.

Yours truly,

Stefano Pruno

STUDY PARTICIPANTS

Study Coordinator	Albert Hebing, Laboratory Manager
Report Preparation	Stefano Pruno, Special Core Analyst/Geologist
Basic Rock Properties	Arno van Schaik, Core Analyst
CMS-300	Core Laboratories (CoreLab), United Kingdom
Sonics	Peter Steenbergen, Special Core Analyst
Wet Chemistry CEC	Arno van Schaik, Core Analyst
Mercury Injection	Ab Coorn, Core Analyst
Formation Resisitivity Factor	Stefano Pruno, Special Core Analyst/Geologist
Formation Resistivity Index	Stefano Pruno, Special Core Analyst/Geologist
Relative Permeability	Jurriaan Nortier, Special Core Analyst/Geologist
Report Review	Albert Hebing, Laboratory Manager

TABLE OF CONTENTS

1. INTRODUCTION

Wintershall Noordzee B.V. requested PanTerra Geoconsultants B.V. to perform special core analysis (SCAL) on plugs from core 1 of well D12-A2. In this report the special core analysis test methods and results are described and discussed.

PanTerra received Core #1 of Well D12-A2 on 11 July 2003. The cored interval with a total recovered length of 33,30 meters comprises Upper Carboniferous sediments.

o SCAL Program

Thirteen 1.5" diameter plug samples divided in A, B and C sets were drilled from the cores (table 1A). Twelve of these samples from the A and B set were used for special core analysis tests. The SCAL program for these samples is shown in table 1B. CT-scans and images of sample end faces by flatbed scanner were made of the 12 samples used for testing. The images can be found in the Enclosures section.

Petrography was performed upon trim-ends of 13 SCAL plugs. Petrography results have been presented and discussed in geological report no. G488 (August 2004).

NOTE: During course of special core analysis program some degree of halite dissolution was observed for sample S2 and S4, subsequent testing of those samples was cancelled. Some analysis have been carried out for completeness and included in this report, however the application of the core analysis results of samples S2 and S4 might be limited.

2. CORE ANALYSIS PROCEDURES

2.1 Sample Selection, Extraction and Drying

Sample Selection

Sample selection for special core analysis purposes was done by Wintershall Noordzee B.V. Plugging of the samples was performed using 2% KCl saturated brine as drill bit lubricant to prevent clay damage. Each plug, except those of the C set, was trimmed to form a cylindrical sample and the trim-ends were bagged, labelled and stored for possible further analyses. SCAL samples of the A and B set that were not used for analysis were stored under brine.

SCAL samples belonging to the C set were wrapped in cling-film and aluminium-foil and then stored for possible rock strength testing.

Extraction

The SCAL plugs were placed in a soxhlet apparatus and cleaned using an azeotropic mixture of methanol, chloroform and water to remove any residual hydrocarbons and (formation water) salts. The plugs were considered to be cleaned of salts when the solvent in direct contact with the core plugs was free from precipitate when tested with 10% silver nitrate solution, and clean of residual hydrocarbons when the core plugs did not fluorescence when viewed under ultra-violet light.

Drying

The SCAL samples were dried in a humidity oven at 60°C and 45% relative humidity, until constant weight was achieved. Before analysis of basic properties the samples were cooled to room temperature in a dessicator without silica gel.

2.2 Porosity, Permeability and Grain Density

Porosity of the samples was determined by direct measurement of grain volume and bulk volume. Grain volume was determined by helium expansion in a Boyle's Law porosimeter. In this method, a reference cell is charged with helium at a pressure of 100 psig, and the helium permitted to expand into a sample chamber containing the test sample. The pressure drop is proportional to the grain volume of the sample, which is determined by reference to a calibration curve of final pressure versus volume for a set of standard steel discs. The grain volume together with the bulk volume, measured by submerging the sample in mercury (Archimedes Law), allows calculation of the porosity.

Grain density is calculated from Boyle's Law using the measured weight of the sample and its grain volume:

$$V_g = \frac{P_{xc}(V_r - V_s) - P_r \cdot V_r}{P_{xc}}$$

where:

V_g = grain volume, ml

P_{xc} = gauge pressure reading (obtained when the helium expands into the sample chamber), psig

V_r = reference volume, in ml

V_s = sample chamber volume, ml

P_r = initial reference pressure, 100 psig

The effective sample porosity fraction is defined as:

$$\phi = \frac{V_b - V_g}{V_b}$$

where:

ϕ = porosity, fraction

V_g = grain volume, ml

V_b = bulk volume, ml

Permeability of the samples was determined by use of a nitrogen permeameter. The test samples were mounted in a "Hassler" type core holder at a confining pressure of 400 psig. Steady state flow was established through the sample and flow rate, pressure differential and temperature recorded. These were used in conjunction with the callipered length and diameter to compute permeability from Darcy's equation:

$$k_g = \frac{\mu \cdot Q_b \cdot P_b \cdot L}{A \cdot D_p \cdot P_m}$$

where:

k_g = gas permeability, darcies

μ = gas viscosity, centipoise

Q_b = gas flow rate, ml/s

P_m = mean pore pressure, atmospheres = $\frac{1}{2}(P_1 + P_2)$

P_b = base or atmospheric pressure in absolute units, atmospheres

D_p = differential pressure in absolute units, atmospheres = $(P_1 - P_2)$

L = plug sample length, cm

A = plug sample cross-sectional area, cm²

P_1, P_2 = upstream and downstream pressure in core sample in absolute units, atmospheres

Klinkenberg (Gas-Slippage Corrected) Permeability

K_l (<400mD) = $0.68 \bullet K_g^{1.06}$

K_l (>400mD) = $K_g (((K_g / 1000) \bullet 0.005) + 0.95)$

where:

K_l = Klinkenberg gas-slippage corrected gas permeability, darcies

Porosity, permeability and grain density results of the core plugs are shown in table 2. A semi-log plot of porosity versus permeability is shown in figure 1.

2.3 X-ray tomography (CT-Scan)

The samples were scanned using a Siemens Somatom AR. Two cross-sectional scans, 90 degrees opposite each other, in the length direction of the plug (direction A and B). The images were used to reveal internal structures, heterogeneities and to assess fractures.

The principle of the scanner is that a beam of X-rays of known intensity penetrates the core and the outgoing beam is measured. The intensity difference equals the total attenuation of the X-rays in the core and is related to the density. Rotation of the tube and detector assembly around the core yields a large number of relations with respect to intensity differences and X-ray attenuation coefficients. The computer calculates the attenuation coefficients for the respective sections of the core. The attenuation coefficients are visualised in gradations of black and white and are displayed on a monitor. High density yields light colours, lower density dark colours.

The images are included in the Enclosures section.

2.4 Brine Properties and Sample Saturation

Synthetic formation brine used for sample saturation was prepared according to the composition supplied by Wintershall Noordzee BV. The composition can be found in table 3.

Saturation

The clean dry samples were weighed and placed in a sealed container and evacuated for a minimum period of eight hours.

The container was then filled with synthetic formation brine, which was prepared according to the supplied compositions, and pressurized to 2000 psig. This pressure was maintained for a period of 24 hours after which pressure was slowly released. Samples were subsequently removed from the container and weighed. The difference between the dry sample and saturated sample weight is a measure of the volume of brine in each core sample.

Saturation was checked by:

$$S_w = \frac{(M_{sat} - M_{dry})}{\rho_{brine}} \cdot \frac{1}{V_p} \cdot 100$$

where:

S_w = brine saturation, fraction

V_p = helium pore volume, ml

M_{sat} = weight of sample saturated with brine, g

M_{dry} = weight of sample dry, g

ρ_{brine} = density of brine saturant, g/ml

Samples were considered fully saturated when S_w was 98-102%.

2.5 Porosity and Permeability at Confining Pressure

The CMS-300 is an automated permeameter / porosimeter that measures permeability by a transient pressure fall off technique. Helium flows to its hydrostatically - stressed sample holder from one of five reservoirs of accurately known volume and is vented to atmospheric pressure. The upstream pressure, which is initially about 240 psig, is monitored as a function of time by a microcomputer. Instantaneous flow rates are calculated from the known reservoir volume and the rate of pressure decay. Instantaneous pressure differences across the plug are numerically equal to the upstream pressure readings. Corrections are made for the non-constant mass flow rate, due to the pressure transient.

A pneumatic stress intensifier provides axial stress, which is an integral part of the lower end plug. A radial stress of equal magnitude is delivered by oil pressure on the rubber sleeve of the sample holder from a pneumatically - drive pressure intensifier. The minimum desirable confining stress is 800 psi, and the maximum is 10,000 psi.
Because wide ranges of flow velocities, gas densities, and mean pore pressures are obtained from a single transient pressure fall off, the Klinkenberg (or slip-corrected) permeability,, the Klinkenberg gas slippage factor (b_{He}) and the Forchheimer inertial resistance coefficient (can all be calculated directly from the time-pressure data through the Forchheimer equation, which has been integrated with respect to the length of the core plug at each time interval of the measurement. Note that the Darcy equation is a special limiting case of the Forchheimer equation when the inertial flow resistance of a porous medium to a fluid is negligible compared to its viscous flow resistance.

Porosity and permeability results for seven 1.5” diameter SCAL samples are shown in table 4. Porosity and permeability reduction with confining pressure is plotted on figures 2 and 3, respectively.

2.6 Ultra-sonic Pulse Velocity Vp and Vs

Ultrasonic pulse velocities measurements were conducted on 5 cylindrical SCAL plugs to determine their P- and S-wave velocities, and hence their dynamic elastic constants [1,2]. All measurements were performed twice: firstly under dry condition at room temperature, zero pore pressure and at a net hydrostatic confining pressure of 6500 psi, secondly under fully brine saturated conditions at the same temperature and pressures.

The plugs were end-ground to improve the ultrasonic coupling between the transducers and the sample[1] and to minimise adverse end-effects during the loading of the samples.[3] Prior to testing, the saturated bulk densities g_{Sat} of the samples were determined by measurement and weighing[4].

Hydrostatic loading of the plugs during the measurements was achieved using Hoek-type cell in conjunction with a hydraulic pressure intensifier to apply the lateral load, and using a 10,000 psig capacity hydraulic loading frame to apply the axial loading. The samples were located within the cell, and axial load on the samples was applied via steel platens adjacent to their prepared end-faces. Axial load on the samples and lateral confinement were measured using calibrated pressure transducers.

A direct pulse-transmission technique along the axes of the plugs was employed for the ultrasonic measurements, using both P- and S-waves. A matching load-bearing piezoelectric transmitter and its receiver were located directly opposite one another against the steel platens adjacent to the prepared end-faces of the plugs. Ultrasonic coupling was further facilitated by use of lead foil between the samples and the loading platens, and by use of an organic couplant between the transducer housings and the steel loading platens. The transducers, having frequency responses of nominal 590-700 kHz, were used in conjunction with a matching CNS PUNDIT system, which provided the pulse excitation and a digital timing unit with resolution to 0.1 msec, and with a digital oscilloscope with a time-axis resolution to 0.0625 μsec. This enabled detection of first arrivals of the P- and S-wave signals, and the P- and S-wave travel times determined for each sample were corrected for travel through the transducers and steel platens, determined by taking measurements with the transducers and platens in face to face contact with lead foil couplant under a confining pressure of 6500 psig. From the measurements of bulk densities g_{Sat} and corrected P- and S-wave velocities V_P and V_S, dynamic values of Young's modulus E (GPa), shear modulus G (GPa), bulk modulus K (GPa) and Poisson's ratio ν were computed for the plugs assuming them to be isotropic.

Test results are presented in table 5. A plot of acoustic velocity versus porosity is shown in figure 4.

---

[1] American Society for Testing and Materials (1976); ASTM D2845-69 : Laboratory determination of pulse velocities and ultrasonic elastic constants of rock

[2] International Society for Rock Mechanics (1978); Suggested Methods for Determining Sound Velocity; Int. J. Rock Mech. Min. Sci. & Geomech. Abstr., Vol. 15, No. 2, pp. 53-58, 1978

[3] International Society for Rock Mechanics (1983); Suggested Methods for Determining the Strength of Rock Materials in Triaxial Compression : Revised Version; Int. J. Rock Mech. Min. Sci. & Geomech. Abstr., Vol. 20, No. 6, pp. 283-290, 1983

[4] International Society for Rock Mechanics (1979); Suggested Methods for Determining Water Content, Porosity, Density, Adsorption and Related Properties and Swelling and Slake-Durability Index Properties; Int. J. Rock Mech. Min. Sci. & Geomech. Abstr., Vol. 16, No. 2, pp. 141-156, 1979

2.7 Cation Exchange Capacity and Qv

Cationic exchange capacity was performed on trim-ends of 5 SCAL samples by a conductometric titration. The initial step involves the boiling of approximately 10 grams of sample in de-ionised water for 4 hours to release the clay particles. Hereafter, the samples were saturated with excess barium chloride. The excess barium ions, that are not replacing the cations on the surface of the clay minerals, were removed by repeated centrifugation prior to performing the conductometric titration. During titration (with magnesium sulphate solution of known concentration), the magnesium sulphate initially reacts with barium, which occupies exchange sites on the clay particles. The conductivity of the solution is monitored throughout the titration. During the initial reaction stage the conductivity of the solution remains almost constant. When the reaction is complete (equivalence point), the addition of further magnesium sulphate causes the conductivity to increase. Plotting the conductivity vs. volume of magnesium sulphate enables determination of this equivalence point, the end point of the reaction. This value is obtained in milli-equivalents (meq) of magnesium sulphate, therefore, cationic exchange capacity in milli-equivalents per 100 grams can be calculated by:

$$\mathrm{CEC\,(meq/100g)} = \frac{\text{reaction endpoint (meq)} \cdot \text{normality of } MgSO_4 \cdot 100}{\text{Sample Weight (g)}}$$

Pore volume was calculated from helium porosity data of the plugs and this pore volume enabled the calculation of Q_v by:

$$Q_v\,(\mathrm{meq/ml}) = \frac{\text{reaction endpoint (meq)} \cdot \text{normality of } MgSO_4}{\text{Sample Pore Volume (ml)}}$$

Table 6 and figure 5 show CEC and Q_v results for the SCAL samples.

2.8 High Pressure Mercury Injection

Five clean, dry samples were selected for high pressure mercury injection

The samples were weighed and each placed in the bulb of a penetrometer, which was loaded into the low pressure chamber of a Micromeretics Autopore III 9420 porosimeter.
The penetrometer was evacuated to a pressure of less than 30 μm of mercury, and then filled with mercury until a pressure of 1 psia.
During the drainage phase mercury, being the non-wetting phase, was injected into the core plug at increasing incremental pressures from 1 to 30 psia. At each pressure step, mercury intrusion was monitored and constant pressure was maintained. Equilibrium was identified when the rate of intrusion dropped below 0.001 μL/g/sec. Pressure and total intruded mercury volume at equilibrium were recorded.

After equilibrium had been established injection pressure was reduced to atmospheric and the penetrometer was removed and weighed with the sample and the mercury in place. It was then loaded into a high pressure chamber of the Autopore system.

For drainage only, and calculation of the pore size distribution, the cumulative volume of mercury injected is increased by incremental pressure changes up to a maximum of approximately 60,000 psia with data being recorded at each pressure as described in the paragraph above.

Pore size distribution data were then calculated. Values used: Contact angle air-mercury: 140^{o}, interfacial tension air-mercury: 480 dynes/cm.

Mercury saturations were calculated as a percentage of the pore volume at each pressure. The pore volume used for calculation of mercury saturation was obtained from the maximum intrusion volume.

Calculation of mercury injection data:

Sample weight, sample and penetrometer weights with and without mercury were used to calculate grain density and bulk density.

Volumes of mercury at each injection pressure were recorded.

The cumulative mercury intrusion was plotted against the injection pressure. Initial intrusion at low pressure is the result of mercury conforming to the surface irregularities of the sample. These irregularities have been created during core plugging and handling and are not representative of the sample's pore structure. The threshold pressure at which injection into the pore structure begins is identified by an increase in the gradient of this plot. Cumulative injection up to this injection pressure is subtracted as surface porosity from measured data before subsequent calculations are made.
Cumulative volumes of mercury injected are expressed as a fraction of the initial pore volume calculated from the re-determined base data.

At a mercury displacement pressure, Pc, the minimum size of pore, r, which can be filled by mercury is given by:

$$r = \frac{2\sigma \cdot \cos\theta \cdot C}{Pc}$$

where:
r = pore throat radius, μm
σ = interfacial tension between air and mercury, dynes/cm (480)
θ = contact angle between air and mercury, degrees (140)
Pc = capillary pressure, psia
C = conversion constant (0.145)

Using this relationship, a graph of fraction of pore volume injected versus log pore throat diameter can be constructed. The differential of this gives the pore size distribution.

$$Pore\ size\ distribution\ (PSD) = \frac{\delta\ v}{\delta\ log(r)}$$

where:
$\delta\ v$ = change in mercury filled pore volume (saturation), fraction of the bulk volume.
r = pore throat radius, μm

Air-brine capillary pressure (laboratory) data can be obtained from air-mercury data by the following conversion:

$$Pc_{o\_b} = Pc_{a\_Hg} \cdot \frac{\sigma_2 \cdot \cos\theta_2}{\sigma_1 \cdot \cos\theta_1}$$

where :
$Pc_{o\text{-}b}$ = oil-brine capillary pressure (reservoir), psia
$Pc_{a\text{-}Hg}$ = air-mercury capillary pressure, psia
σ_2 = interfacial tension between oil and brine (reservoir), dynes/cm (30)
θ_2 = contact angle between oil and brine (reservoir), degrees (30)
σ_1 = interfacial tension between air and mercury, dynes/cm (480)
θ_1 = contact angle between air and mercury, degrees (140)

The mean hydraulic radius, (MHR), is the average pore throat size of the sample and is given by:

$$\mathrm{MHR} = \sqrt{\left(\sum_{i=0}^{n} r_i^{\,2} \cdot \Delta S_i\right)}$$

where :
$\Delta S_i = \left|S_{i+1} - S_{i-1}\right|$
S = mercury saturation, fraction of pore volume
r_i = pore throat radius

Theoretical permeability, Kt, of a sample with a given pore size distribution is calculated using the following equation:

$$Kt_j = \frac{125}{(FRF \cdot Kt_{\max})} \cdot \sum_{j=0}^{n} r_j^{\,2} \cdot \Delta S_j$$

or

$$Kt_i = 125 \cdot MHR^2 \cdot \phi_i^{\,2}$$

where:
FRF = Formation resistivity factor
ϕ = Porosity, (fraction)
Kt_j has been normalised such that the maximum value is 1.0.

Cumulative permeability was calculated from:

$$Cumulative\ K_i = 1 - Kt_i$$

Calculation of Pore Throat Sorting (PTS):

The distribution of pore throat sizes in a plug sample can be calculated from mercury injection data. Pore throat sorting (PTS) is reflected in a single number ranging from 1.0 (perfect sorting) to 8.0 (essentially no sorting). PTS is calculated as follows:

$$PTS = \sqrt{\frac{3rd}{1st}}$$

Where 1st and 3rd are the first and third quartile pressures obtained from the capillary pressure curve and reflect the 25 and 75% mercury saturation, respectively.

Calculation of Reservoir Grade:

Reservoir grade indicates the reservoir quality of a rock and ranges from 0 (best quality) to 100 (lowest quality). RG is the percentage of linear area integrated under the capillary pressure curve and is calculated by plotting the data linearly and planimetering the area below the curve.

Usage of pore size distribution graphs (figures 6-10):

Three related parameters are plotted against pore size, which appears on the horizontal, logarithmic scale. These are:

a) Cumulative mercury saturation
b) Pore size distribution
c) Cumulative theoretical permeability (Kt)

These parameters are plotted on the vertical scale as fractions.

The cumulative mercury saturation is plotted as a fraction of the total intrusion volume vs. pore size, and is shown as a solid line with individual points indicated by black squares. At the maximum intrusion pressure of 60,000 psia, the total volume of pores accessed is regarded as the maximum volume available. All plots will therefore have a final saturation of 100% (1.00 fractional). The same data is plotted against pressure on the accompanying capillary pressure plots. As a rule of thumb, the further to the right on the plot the saturation increases, the lower the equivalent S_{wir} value will be, indicating better rock quality, as a fraction of the pore size.

The pore size distribution is plotted as a fraction of the maximum incremental volume injected. This plot gives useful information about the relative abundance of pore sizes. If a single "peak" is plotted with a general low "background", then a restricted pore size range dominates. A "plateau" of relatively high values will indicate there is no dominant pore size. The position of such peaks is important in explaining the petrophysical properties of samples. A sample with a peak shifted to the left will have a predominance of micro pores, while a plateau indicates a more even distribution of macro, meso and micro pores.

The cumulative theoretical permeability (Kt), plotted as a blue line, shows the relative contribution of pores to the permeability. The actual value reported for Kt is accurate to within one order of magnitude and is dependant on the quality of the sample used (e.g. a carefully prepared plug compared with drill cuttings) and the mathematical model used. A more accurate value is derived if Formation Resistivity Factor is used in the calculation of Kt, as it is a good measure of pore tortuosity within a sample. Measured FRF values have been used in this study if available. If not available FRF was calculated from $1/\Phi^m$ by using m = 2. By displaying the data on a plot, it is possible to quickly derive the relative contribution of the pores to the permeability e.g. in sample 110c, 83% of the permeability is controlled by pore throat radius larger than 3 microns. At the same pore throat size, the mercury saturation is approximately 18%. Therefore 18% of the pores are contributing to 83% of the theoretical permeability. As a rule of thumb, the higher the percentage of contributing pores and the higher the pore throat radii, the better the rock reservoir quality.

Table 12 shows a summary of mercury injection data for all samples. The data of the individual samples are shown in tables 7-11 and figures 6-10.

Note: Please note that the pore throat size is given as diameters.

2.9 Formation Resistivity Factor and Porosity Exponent *(m)*

Formation Resistivity Factor at Ambient Temperature and Pressure

Electrical resistivity measurements were done following the full saturation of the appropriate plugs with the synthetic formation brine.

The electrical resistivity of the brine saturated core plugs was measured at ambient conditions on consecutive days until the resistivity value of each sample had stabilised. At this point, the samples were judged to have reached ionic equilibrium with the synthetic formation brine.

The Formation Resistivity Factor ("FRF") at ambient conditions was calculated using the following relationship:

$$FRF = \frac{Ro}{Rw}$$

where:

Ro	=	resistivity of the 100% saturated core plug, Ω.m
Rw	=	resistivity of the formation brine, Ω.m

A composite graph of log Formation Resistivity Factor versus log porosity (ϕ) was made for the suite of samples, (figure 14). The line of best fit through the data points was determined with the least squares regression method - which calculates the best straight line through the set of points on a mathematical basis – and "force fitting" the line through the (1.0, 1.0) point.

The gradient of the resulting line is the Porosity Exponent "m" in accordance with Archie's formula:

$$FRF = \frac{a}{\phi^{m}}$$

where :

a	=	intercept with the Y-axis, (a=1 when the line is fitted through (1,1))
m	=	porosity exponent (or Cementation Exponent)
ϕ	=	porosity (fraction)
FRF	=	Formation Resistivity Factor

Formation Resistivity Factor at Confining Pressure and Ambient Temperature

Following the determination of the Formation Resistivity Factor at ambient conditions, each brine saturated core plug was mounted into a rubber sleeve and confined between stainless steel end platens. Brine saturated capillary contact mat and a platinised disc were placed at the ends of the sleeved sample in order to minimise contact resistance and electrode polarization effects. The stainless steel flow platens and stems were filled with the formation brine in order to prevent any air being introduced into the sample.

The sample-sleeve assembly was loaded into an insulated, hydrostatic confining pressure cell with the upper outlet tube connected to a calibrated micropipette, allowing the measurement of expelled brine volumes and hence of the pore volume reduction.

The required confining pressure was applied using a non-conductive hydraulic oil. Measurements were done at net confining pressure values of 3700 psig.

The amount of expelled brine and the resistivity were measured over the initial 400 psig pressure range in order to determine the pressure where the initial brine displacement due to adjustment of the sleeve to the core plug surface, changed to brine squeeze-out due to pore volume reduction of the sample.

The electrical resistivity measurements were made at the resonance frequency with a Wayne Kerr auto-balancing bridge via connections to the inlet and outlet platen pipes that are in contact with the core end-faces. All the resistivity measurements were corrected for residuals through the open-short compensation technique for the whole frequency range.

The resistivity value that was measured at the point of initiation of pore volume reduction was found to equate with the value measured under ambient conditions.

The confining pressure was then increased to the stipulated value. At each pressure value, resistivity measurements were intermittently made simultaneously with the measurement of the amount of expelled brine until these values stabilised within 2% change. This indicated that ionic and pressure equilibrium had been achieved.

A composite graph of log Formation Resistivity Factor versus log Porosity (ϕ) was made for each selected pressure value and the porosity exponent (m) relating to this graph was determined as described before, (see figures 14 to 15). The porosity change was as “relative pore volume reduction” plotted versus the applied confining pressure, (figure 16).

The FRF measurements and porosity exponents are presented in table 13 and 14.

2.10 Air Brine Capillary Pressure and Saturation Exponent (*n*)

Eight samples were selected for determination of Formation Resistivity Index (FRI) and Saturation Exponent (n) in conjunction with air-brine capillary pressure curves. This involves stepwise de-saturation and measurement of electrical resistance of the samples.

Before de-saturation of the samples the resistivity at fully saturated conditions (R_0) was measured using an ambient resistivity cell connected to a Wayne-Kerr auto balancing bridge. In this cell a core plug sample is clamped between two end-faces by a pneumatic ram at a pressure of 100 psig. Electrical contact between the sample and cell is made using silver screens and silver impregnated rubber on each side of the plug. Resistance, phase angle, frequency and test temperature are then recorded.

After measurement of R_0 the samples were ready for stepwise de-saturation. Therefore a porous semi-permeable ceramic plate was saturated with the same brine as used for sample saturation. The sample plugs were placed on the ceramic plate in the cell, which was housed in a temperature-controlled environment. A paste of diatomaceous earth and brine, separated from the core plug by brine soaked filter paper, was used to ensure good capillary contact between the porous plate and each core sample. On top of each sample a metal screen and lead weight was placed.

After closure of the cell humidified air, being the displacing phase, was introduced into the cell at the starting pressure, which was in this case 1 psig.

Brine that was expelled from the samples, through the porous plate was collected in a container outside the cell. The weight of this container was monitored daily. Sample weight was checked weekly. When sample weights had stabilized the samples were considered to be in saturation equilibrium at applied pressure. At that point they were removed from the cell. Brine saturation in the sample was then calculated from sample weight, pore volume and brine density:

$$S_w = \frac{(M_{sat} - M_{dry})}{\rho_{brine}} \cdot \frac{1}{V_p}$$

where:

S_w = brine saturation, fraction of Vp

V_p = pore volume, ml

M_{sat} = weight of partially saturated sample, g

M_{dry} = weight of sample dry, g

ρ_{brine} = density of brine saturant, g/ml

The samples were then loaded in the ambient resistivity cell connected to a Wayne-Kerr auto balancing bridge to determine electrical resistivity (R_t) of each partially saturated sample. Electrical contact was achieved by using silver screens and silver impregnated rubber on each side of the plug.

The formation resistivity index (FRI) can then be calculated from:

$$FRI = \frac{R_t}{R_o}$$

where:

R_t = True resistivity = resisitivity of partially saturated sample (Ω.m)
R_o = Resistivity of 100% brine saturated sample (Ω.m)

After measurement of the formation resistivity index all samples were returned to the cell and the process was repeated at capillary pressure steps of 1, 4, 12, 55, 130 and 180 psig. At each pressure the samples were allowed to attain equilibrium.

After finishing all pressure steps a plot of log FRI versus log S_w was prepared for each sample and a linear regression fit, forced through the Y intercept of 1, was constructed to fit the data. The Archie saturation exponent (n) was then calculated from the slope of the fitted line:

$$FRI = S_w^{-n}$$

In addition air-brine capillary pressure curves were constructed by plotting saturation versus capillary pressure. A curve was fitted to the data points using the Lambda Equation:

$$S_w = (a+b) \cdot P_c^{(d\phi+e)}$$

where:

P_c = capillary pressure, psig

S_w = brine saturation, fraction of Vp

ϕ = porosity , fraction

a,b,d,e = numeric coefficients

Data can be found in table 15. FRI plots and capillary pressure curves for individual core plugs are shown in figures 18 - 25. Composite FRI and capillary pressure plots are shown in figures 17 and 26.

2.11 Formation Resistivity Index and Saturation Exponent (*n*) at Confining Pressure

Following sample ambient resistivity measurements by porous plate after last capillary pressure step of 180 psig each core plug was mounted into a rubber sleeve and confined between stainless steel end platens. Silver coated screens were placed between the sample and end platens to minimise contact resistance and electrode polarization effects.

The sleeve, containing the sample was then loaded into an insulated, hydrostatic pressure cell and confined to a stress of 6500 psig. Electrical resistivity measurements were then made at resonance frequency until equilibrium has been reached, using a Wayne Kerr auto-balancing bridge via connections to the inlet and outlet platen pipes, which are in contact with the core end-faces.

Formation resistivity index measurements and accompanying saturation exponents are listed in table 16.

2.12 Unsteady-state Gas-Brine Relative Permeability at Ambient Pressure and Temperature Conditions

Two samples were selected for unsteady-state gas-brine relative permeability determination.

Base permeability
The initial step involved specific brine permeability measurement on the individual samples to establish the base permeability to which effective permeability to gas and brine was normalized. Therefore the samples, fully saturated with synthetic formation brine, were loaded vertically into a Hassler type core holder and confined to a pressure of 400 psi. Brine was flowed through the samples at different flow rates while pressure differential and temperature were recorded. Brine permeability was then calculated from Darcy's law for fluid flow through porous media:

$$K_L = \frac{Q \cdot \mu \cdot L}{A \cdot \delta P}$$

Where:

K_L = brine permeability, Darcy, D
Q = brine flow rate, ml/sec
μ = brine viscosity, centipoises, cP
L = sample length, cm
A = sample cross-sectional area, cm^2
δP = pressure differential, atmospheres, atm

Gas-brine unsteady state relative permeability
After determination of the base brine permeability the fully brine saturated samples were loaded vertically in a Hassler type core holder of the relative permeability rig.
Humidified nitrogen gas was flowed through the sample at constant pressure. The inlet test pressure was chosen such that a high flow rate was maintained during the test in order to minimize capillary end-effects. At predetermined gas throughput volumes, volumes of brine produced and time were noted. The test was stopped when endpoint criteria were met. Endpoint criteria that were used are:

1) Gas/brine ratio > 100
2) Gas cut > 99.95%

Where:

$$\text{Gas/brine ratio} = \frac{14.7 \cdot \mu_g \cdot V_g}{\left[14.7 - \left[\frac{\delta P}{2}\right]\right] \cdot \mu_b \cdot V_b}$$

$$\text{And Gas cut} = \frac{V_g}{\left[V_b + V_g\right] \cdot 100}$$

With:

δP = differential pressure, psi

μ_g = gas viscosity, cP

μ_b = brine viscosity, cP

V_g = Incremental gas volume, ml

V_b = Incremental brine volume, ml

14.7 = atmospheric pressure, psi

These endpoint criteria are considered to be reasonable, as by the time these criteria are met the brine production has practically ceased, and relative brine permeability is close to zero. Gas volume throughput was recorded initially in a 50 ml burette and above 50 ml on a wet test meter. Produced brine was collected in a glass measuring tube. After correcting gas volumes for compressibility, relative permeability and brine saturation were calculated using the Jones-Roszelle[5] method, which is applicable to high rate unsteady state experiments performed at constant inlet pressure. This method is an adaptation of the Johnson-Bossler-Naumann[6] method.

The Jones-Roszelle method involves differentiation of the production data, which was done numerically by using a second order Lagrange polynomial. In order to use this method, raw production data have to be smoothed by using analytical functions, either of the Weibull- or MMF-type, depending upon best fit.

Calculation of relative permeability to gas and brine

The initial step consists of the calculation of the gas saturation at the outlet face of the sample. This involves numerical differentiation of volumes of brine produced versus volumes of gas injected:

$$S_{gL} = \overline{S_g} - Q_{gi} \cdot \frac{\delta Q_{bp}}{\delta Q_{gi}}$$

Where:

$\overline{S_g} = Q_{bp} + S_{gi}$ = average gas saturation, fraction

S_{gL} = gas saturation at outlet face of the sample, fraction

Q_{gi} = gas injected, pore volumes

Q_{bp} = brine produced, pore volumes

S_{gi} = initial gas saturation, fraction

$\frac{\delta Q_{bp}}{\delta Q_{gi}} = F_{bL}$ = fractional brine flow at outlet face of the sample

---

[5] **Jones, S.C., and Roszelle, W.O**., "Graphical Techniques for Determining Relative Permeability from Displacement Experiments", JPT, 1978.

[6] **Johnson, E.F., Bossler, D.P. and Naumann, V.O**., "Calculation of Relative Permeability from Displacement Experiments", Trans., AIME (1959) 216.

Brine saturation at the outlet face, S_{wL}, is subsequently calculated by subtracting gas saturation from unity:

$$S_{wL} = 1 - S_{gL}$$

Second, the gas and water fractional flows at the outlet face of the rock sample are calculated:

$$1 - F_{gL} = F_{bL} = \frac{\overline{S_g} - S_{gL}}{Q_{gi}}$$

Where:

F_{gL} = fractional gas flow at outlet face of sample

Then, the effective viscosity, λ_L^{-1}, at the outlet face of the sample must be calculated. Therefore, total flow rate must be calculated firstly, after which differentiation of average effective viscosity against total flow rate results in effective viscosity:

$$\lambda_L^{-1} = \overline{\lambda^{-1}} - Q_{gi} \cdot \frac{\delta \overline{\lambda^{-1}}}{\delta Q_{gi}}$$

Where:

$$\overline{\lambda^{-1}} = \mu_{base} \cdot \frac{[\Delta P / q]}{[\Delta P / q]_{base}} = \text{average effective viscosity}$$

with:

$[\Delta P / q]$ = *ratio of pressure differential to total flow rate during relperm test*

$[\Delta P / q]_{base}$ = *ratio of pressure differential to flow rate during base permeability test*

μ_{base} = *viscosity of brine during base permeability test*

Now average effective viscosity is known, the relative permeability to gas and brine at the outlet face of the sample can be calculated for the whole saturation range by dividing fractional flows multiplied by viscosity, by the effective viscosity:

Gas relative permeability:

$$K_{rG} = \frac{\mu_g \cdot F_{gL}}{\lambda_L^{-1}}$$

Brine relative permeability:

$$K_{rB} = \frac{\mu_b \cdot F_{bL}}{\lambda_L^{-1}}$$

A summary of the relative permeability data is given in table 17. Individual relative permeability data are presented in tables 18 and 19. Endpoint gas permeability presented in these tables is calculated by multiplication of the maximum relative gas permeability with the base brine

permeability. Three graphs (figures 27 and 28) are supplied for each sample as well. Two of them, plotted on normal (a) and logarithmic scale (b), show sample saturation versus relative permeability. The third graph (c) reflects sample saturation versus relative permeability ratio.

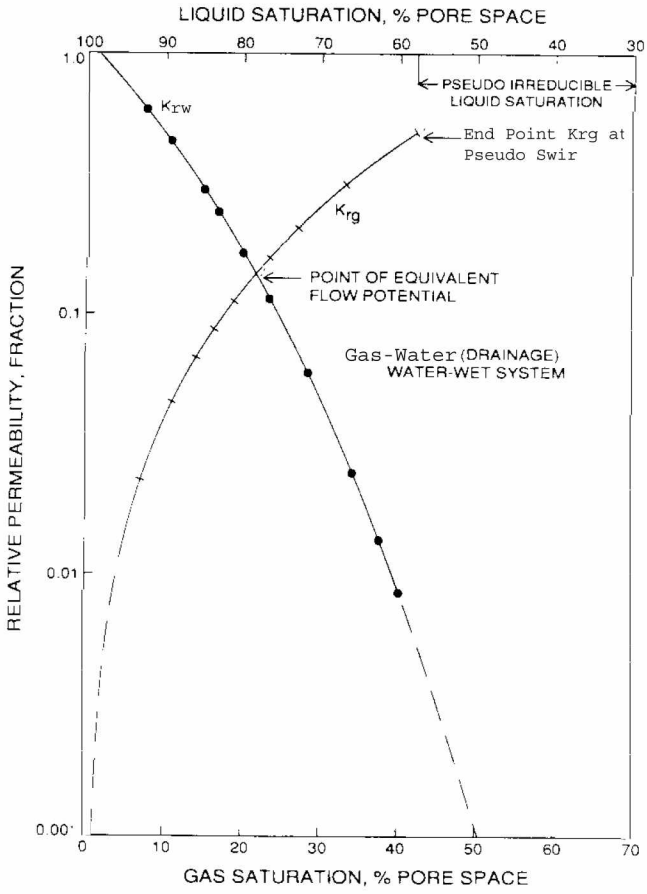

Figure C: A typical gas-water relative permeability relationship

3. DISCUSSION OF RESULTS

Porosity, Permeability, and Grain Density
Figure 1 shows that a typical linear relation exists between porosity and permeability. Sample S2, S4 (halite dissolution) and S36 (fractured) were excluded from regression line calculation. In general permeability increases with increasing porosity. Grain density ranges from 2.63 to 2.79 g/ml.(table 2)

Two porosity-permeability groups can be distinguished.

The first group from the Upper Carboniferous comprises samples S2, S4, channel sandstone deposits, very fine grained with poor sorting and presence of halite cement; samples S18, S22 (subarkose) and S27 (mudstone/siltstone) comprises crevasse splay deposit and well drained floodplain, except for sample S36 that was deposited in a ferralithic soil environment. This group shows very poor to poor reservoir properties.

The second group comprises samples S110, S112, S114, S118, S126, S127 and S128 from the Upper Carboniferous that consists of channel sandstone deposits (sublitharenite and quartz arenite). These fine grained sandstones with moderately-good sorting, have the largest authigenic clay content shows moderate-poor reservoir properties.

(refer to PanTerra Geological Report G488, August 2004)

Porosity and Unsteady State Gas Permeability at Confining Pressure
Figure 2 and 3 show that porosity and permeability reduction under increased confining pressure conditions is dependent upon sample porosity, permeability. The lower the porosity and permeability values the higher the reduction. Sample S22A, S27B and S36B are more sensitive for stress showing higher porosity and permeability reduction at 3700 psig hydrostatic confining pressure. Sample 36B (siltstone) shows small microfractures that probably could affect permeability and porosity behaviour with stress. (see table 4)

Acoustic Velocity
Samples S112B and S118B from the lower part of the channel sandstone deposits, with the better reservoir properties, show lower acoustic velocity and dynamic modules at 3700 psig confining pressure compared with the other samples. (table 5)

Cation Exchange Capacity and Qv
Figure 5 shows a trend of increasing Qv with decreasing porosity. The relation found is $Qv = 614.04 * (1/porosity)^{3.1831}$ with a correlation coefficient of 0.953. As expected the Qv is largest for sample S22A (subarkose) and S36A (siltstone) due to the presence of abundant clay. (see table 6)

High Pressure Mercury Injection
All tested samples show very different pore size distribution curves.
Sample 22 show a pore size distribution curve with a broad peak in the sub-micro and nano pore region.
Sample 27 (mudstone/siltstone) is characterized by a peak situated in the sub nano pore region.
Sample 114 have a pore size distribution dominated by very sharp peak located around 3 micron pore throat diameter and sloping away to the micro-pores region.

Sample 126, fine grained and laminated (cross-bedded) quartz arenite show a bimodal pore size distribution in the regions micro and nano pores (or nano-ports).
Sample 110c shows a well defined peak rising in the meso-pores region than sloping away more gradually to a broad low peak in the sub-micro pore regions. (see figures 6 to 10)
From figures 11-13 it appears that a good relationship exist between Klinkenberg permeability and threshold pressure, theoretical permeability and mean hydraulic radius. Samples 110c and 114 a have threshold pressure between 15 and 30 psia showing the largest mean hydraulic radius of 1.410 and 0.970 micron respectively, samples 3 and 16 show mean hydraulic radius of 0.469 and 0.297 micron respectively and a better reservoir grade of 33. Sample 27 (very fine siltstone) show the smallest mean hydraulic radius of 0.013 micron and the higher threshold pressure of 761.8 psia. (see table 12)

Formation Resistivity Factor and Porosity Exponent (m)
Figure 15 shows composite plots of Formation Resistivity Factor versus porosity at 3700 psig confining pressure. The composite porosity exponent by forced fit regression is 2.04. The porosity exponent from the selected set samples at 3700 psig confining pressure ranges from 1.92 to 2.14 indicative of a well cemented sandstone, except for sample S36A (siltstone) which present a lower m values of 1.79 probably related to the presence of abundant clay. Porosity reduction during testing was in general smaller for samples S2A and S36A which is in accordance with the porosity at confining pressure results.(see tables 13 and 14)

Air-Brine Capillary Pressure and Saturation Exponent (n)
The saturation exponents (n) measured at ambient conditions vary within the range 1.62–1.87 for samples S112A, S117A, S118A, S127A and S128A with better reservoir properties and between 1.21 and 1.44 for samples S2A and S4 having the lower reservoir quality. The values of "n" for samples S2A and S4 could also be influenced by halite dissolution experienced during testing. The individual Sw-RI plots show that relationships are linear for all the samples.
The capillary pressure results (figure 17) for the channel deposits samples with better reservoir properties show Swr values between 30.9% and 40.2%. Samples S2A and S4 with lower reservoir properties have lower Swr of 20.5% and 15.3% respectively and probably related to halite cement dissolution. Sample S18 due to low de-saturation show a too high "n" value of 7.03, we would recommend not to use this value for log analysis. (see table 15)

Formation Resistivity Index and Saturation Exponent (n) at Confining Pressure
The saturation exponents (n) measured at 3700 psig confining pressure vary between 1.03–1.68, indicating a reduction of the "n" values for all samples with increasing confining pressure, probably related to the presence of abundant authigenic clay (see table 16).

Unsteady-state Gas-Brine Relative Permeability
Endpoint brine saturation of the samples are in the range 46.4-62.8 %. Gas and brine permeability values are similar indicating less brine-rock interactions. Endpoint gas relative permeability varies within the range 1.077 – 0.734 (fraction).(see table 17 and figures 27 and 28).
End point saturation from relative permeability test may differ from those obtained from capillary pressure by porous plate and continuous injection measurements. The inhomogeneous nature of some samples, high gas-brine mobility ratio, early gas break-through and possibly capillary end effects, can result in termination of the unsteady-state relative permeability test at relatively (too high) end point saturations. If this is the cause Swir as obtained from porous plate capillary pressure test is more representative to the Swir in the reservoir.

4 LIST OF TABLES

5 LIST OF FIGURES